Heliyon 10 (2024) e28608

Contents lists available at ScienceDirect

Heliyon

journal homepage: www.cell.com/heliyon

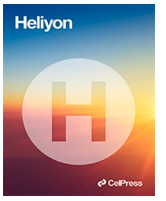

Research article

Endoplasmic reticulum stress and death receptor-mediated apoptosis in the neuronal differentiation of adult adipose-derived stromal cells

Pingshu Zhang [a,b,1], Wen Li [a,b,1], Xinyue Zheng [a,b], Hongjie Luo [a,b], Qing Liu [a,b], Qingxi Long [a,b], Qi Yan [a,b], Xiaodong Yuan [a,*]

[a] Department of Neurology of Kailuan General Hospital Affiliated North China University of Science and Technology, China
[b] Hebei Provincial Key Laboratory of Neurobiological Function, China

ARTICLE INFO

Keywords:
Adipose-derived stromal cells
Apoptosis
Death receptors
Endoplasmic reticulum stress
Induction
Neurons

ABSTRACT

Apoptosis is the primary cause of cell death in the differentiation of Adipose-derived stromal cells (ADSCs) into neurons. However, the relationship between endoplasmic reticulum stress (ERS) and death receptor-mediated apoptosis in ADSC-induced neuronal differentiation is not clear. ADSCs were isolated and induced to differentiate into neurons using β-mercaptoethanol. The expression of neuron-specific enolase (NSE), GRP94, CHOP, Fas/FasL, TNFR1/TNF-α, DR5/TRAIL, Caspase8, and Caspase3 in ADSCs was examined using immunocytochemistry and Western blotting before induction, during pre-induction, and after induction. Transmission electron microscopy (TEM) was used to observe changes in the morphology of the endoplasmic reticulum (ER), and the MTT assay was employed to measure cell viability in the uninduced and induced groups. Additionally, the number of apoptotic cells during the induction process was measured using flow cytometry with Annexin V/PI. With increasing induction time, the positive expression rates of CHOP, Fas/FasL, Caspase8, Caspase-3, and NSE gradually increased, while the positive expression rate of GRP94 decreased. TNFR1/TNF-α and DR5/TRAIL peaked at 5 h post-induction and then decreased at 8 h. TEM revealed swelling and expansion of the ER, vacuolar changes, and degranulation in cells. The MTT assay showed a gradual decrease in the absorbance of surviving cells in all groups. Flow cytometry indicated an increasing rate of apoptosis in cells. Therefore, ERS in the normal culture and growth of ADSCs, manifesting as enhanced unfolded protein response (UPR), maintains the normal survival of ADSCs. However, in the process of ADSC-induced differentiation into neurons, ERS and death receptor-mediated apoptosis are significant causes of cell death.

Abbreviations: ADSCs, adipose-derived stromal cells; DAB, 3,3′-diaminobenzidine; DMSO, dimethyl sulfoxide; DD, death domain; DED, death effector domain; DISC, death-inducing signaling complex; ER, endoplasmic reticulum; ERS, endoplasmic reticulum stress; FBS, fetal bovine serum; FADD, fas-associated death domain protein; NSE, neuron-specific enolase; OD, optical density; PBS, phosphate buffer solution; TRADD, TNFR1-associated death structural domain protein; TEM, transmission electron microscopy; UPR, unfolded protein response.

* Corresponding author. Department of Neurology, Kailuan General Hospital affiliated North China University of Science and Technology;addresses:57 Xinhua East Road, Lubei District, Tangshan city, Hebei Province China,063000:

E-mail address: yxd69@sohu.com (X. Yuan).

[1] pingshu Zhang and Wen Li Joint first author.

https://doi.org/10.1016/j.heliyon.2024.e28608
Received 22 October 2023; Received in revised form 20 March 2024; Accepted 21 March 2024
Available online 26 March 2024

1. Introduction

In 2001, Zuk et al. successfully isolated and cultured Adipose-derived stromal cells (ADSCs) from adult adipose aspirates and discovered that they could be induced in vitro to differentiate not only into adipocytes and osteoblasts, which are mesodermal in origin but also across germ layers into neuronal cells [1]. In 2004, Safford et al. successfully induced the differentiation of ADSCs into neurons and astrocytes in vitro [2]. Due to the advantages of ADSCs, such as easy clinical availability, simple harvesting procedures, and robust proliferative capacity, they have attracted widespread attention from researchers [3–6]. Our preliminary studies found that these ADSC-induced differentiated 5 h neurons possess typical morphological, phenotypic, ultrastructural, and electrophysiological characteristics of neurons [7–9]. However, during this induction process, the cell death rate is high, resulting in a low yield of target cells, insufficient for further research and applications. Studies indicate that mitochondrial pathway-mediated apoptosis is a significant cause of cell death during the in vitro induction of ADSCs into neurons [10,11]. Currently, apoptosis is mainly mediated through three pathways: mitochondrial pathway, endoplasmic reticulum stress (ERS) pathway, and death receptor pathway. Dysregulation of endoplasmic reticulum (ER) homeostasis leads to ERS [12]. The roles of ERS and death receptor-mediated apoptosis in the process of ADSC-induced neuronal differentiation are not well understood. By analyzing the effects of the ERS pathway and the three main death receptor signaling pathways (Fas/FasL, TNFR1/TNF-α, DR5/TRAIL) in the ADSC induction process to neurons, we aim to investigate the causes and mechanisms leading to cell death during this induction response. This will further refine the induction protocol, improve response efficiency, and yield a greater number of ADSC-derived neurons.

2. Materials and methods

2.1. Extraction and cultivation of adult ADSCs and induction of neuronal differentiation

Subcutaneous adipose tissue was extracted from adult volunteers without endocrine and hematological diseases using a needle aspiration method [13]. Following the experimental methods of Lu et al. [11], ADSCs were extracted formed into single-cell suspension and passaged at a ratio of 1:2. When the cell growth reached 70%–80% confluence, the medium was removed and the and pre-induction solution (10 mL FBS, 85 mL high-glucose DMEM, and 7uL β-mercaptoethanol per 100 mL) were added and incubated for 24 h. Afterward, the pre-induction solution was discarded, cells were rinsed three times with saline, and the formal induction solution (100 mL high-glucose DMEM and 35uL β-mercaptoethanol per 100 mL) was added for cultivation. Observation time points during the induction process were set at 1 h, 3 h, 5 h, and 8 h groups. An inverted contrast microscope (Olympus, Japan) was used to observe morphological changes in the cells.

2.2. Expression of NSE/GRP94/CHOP/Fas/FasL/TNFR1/TNF-α/DR5/TRAIL/Caspase8/Caspase3 in cells during induction detected by immunocytochemistry

The uninduced, pre-induced, and induced cells for 1 h, 3 h, 5 h, and 8 h were crawled according to the standard IHC procedure. The cells were permeabilized with 0.1% Triton-X-100 for 10 min, followed by incubation with 3% H_2O_2 for 10 min. They were incubated with diluted primary antibodies: NSE (1:100; EPITOMICS, USA), GRP94 and GHOP (all 1:100; Affinity, USA), Fas, FasL TNFR1, TNF-α, DR5, TRAIL and Caspase8 (all 1:200; Affinity, USA), Caspase3 (1:100; Beijing Zhongshan Golden Bridge, China) overnight at 4 °C. Cells were then incubated with goat anti-rabbit/mouse polyclonal secondary antibody (1:200; Beijing Zhongshan Golden Bridge, China) at 37 °C for 30 min. The cells were then developed with 3,3′-diaminobenzidine (DAB) (Beijing Zhongshan Golden Bridge, China) and stained. Under light microscope (Olympus, Japan) high magnification (× 100). Positive expression cells were identified by the presence of brown-yellow coloration in the cytoplasm or cell membrane, while cells without any coloration were considered negatively expressing cells. This count was performed 5 times in different fields for each sample, and 3 samples were observed in total.

2.3. Western blot detection of NSE/GRP94/CHOP/Fas/FasL/TNFR1/TNF-α/DR5/TRAIL/Caspase8/Caspase3 expression during induction

Cells from each time group were added 100 μL of cell buffer and collected in 1.5 mL EP tubes. Protein concentration in the samples was quantified using the BCA method. The samples were heated in a 100 °C water bath for 5 min to denature the proteins. For each sample, 20 μg of protein was subjected to polyacrylamide gel electrophoresis. The electrophoresis was conducted at 90 V for 90 min, followed by transferring the target bands from the gel to a PVDF membrane under ice-water bath conditions. The primary antibody solutions: NSE (1:1000; EPITOMICS, USA), GRP94 (1:100; Affinity, USA), GHOP, Fas, FasL, TNFR1, TNF-α, DR5, TRAIL and Caspase8 (all 1:1000; Affinity, USA), Caspase3 (1:100; Beijing Zhongshan, China) and β-actin (1:5000; rabbit monoclonal antibody, China) were added and incubated overnight at 4 °C, and the membranes were washed with TBST. Corresponding goat anti-rabbit/mouse secondary antibody (1:5000; Beijing Zhongshan Golden Bridge, China) was added and incubated, followed by washing with TBST. The bands were scanned using a scanner, and the optical density of each band was analyzed using Image J software. Each experiment was repeated three times.

2.4. Ultrastructural features of the ER in control and induced 5 h neurons observed by transmission electron microscopy (TEM)

Samples from the logarithmic growth phase control group and neurons induced for 5 h were taken. The cells were completely

digested with trypsin-EDTA, and the digestion was stopped with a culture medium. The samples were then centrifuged at 4 °C at 1000 rpm for 5 min, and the supernatant was discarded. The cells were resuspended in a complete culture medium, homogenized, and centrifuged again at 4 °C at 1000 rpm for 5 min, discarding the supernatant. The cells were fixed with 2.5% glutaraldehyde for over 3 h and 1% osmium tetroxide for 1 h at 4 °C. After fixation, the samples were washed three times with PBS, each time for 15 min. The cells were pre-stained with 0.5% uranyl acetate overnight at room temperature on a shaker. This was followed by dehydration in propylene oxide and embedding in epoxy resin. Ultrathin sections were prepared using an ultramicrotome. The sections were then doubly stained with 2% uranyl acetate and lead citrate and observed and photographed under the TEM.

2.5. MTT assay to detect the growth status of each group of cells

Digest the 3rd to 5th generation ADSCs to prepare a cell suspension, and seed the cells at a density of 1×10^5 cells per well in a 12-well plate. The inducer is added to set up different groups: uninduced, pre-induced, and induced at 1 h, 3 h, 5 h, and 8 h. Each group has five replicate wells. After induction, 100 μL of 5 g/L MTT working solution (Sigma USA) was added to each well and incubated at 37 °C for 4 h. The liquid in the wells was then discarded, and 1000 μL of dimethyl sulfoxide (DMSO) (Solarbio Beijing) was added to each well. The plates were shaken at low speed for 15 min. Next, 100 μL from each well was transferred to a 96-well plate. The absorbance (optical density, OD value) of each well was measured at 490 nm using an ELISA (BID-RAD USA). The cell growth curve was plotted with time on the x-axis and OD values.

2.6. Flow cytometry annexin V/PI double staining method for quantitative detection of cell apoptosis

Cells from the uninduced, pre-induced, and induced 1 h, 3 h, 5 h, and 8 h groups are collected following trypsin-EDTA digestion. The cell concentration was adjusted to 1×10^6/mL to prepare a single-cell suspension. The cells were centrifuged at 1000 rpm for 5 min, and the supernatant was discarded. The cells were then resuspended in 1 mL of PBS, centrifuged again at 1000 rpm for 5 min, and the supernatant was discarded. 195 μL of Buffer solution and 5 μL of Annexin V staining solution are added to resuspend the cells. The mixture was incubated at room temperature for 10–15 min, then centrifuged at 1000 rpm for 5 min, and the supernatant was discarded. Next, 190 μL of Buffer solution and 10 μL of PI staining solution are added. The cells were kept in the dark and analyzed within 1 h using a flow cytometer. Each experiment was repeated three times.

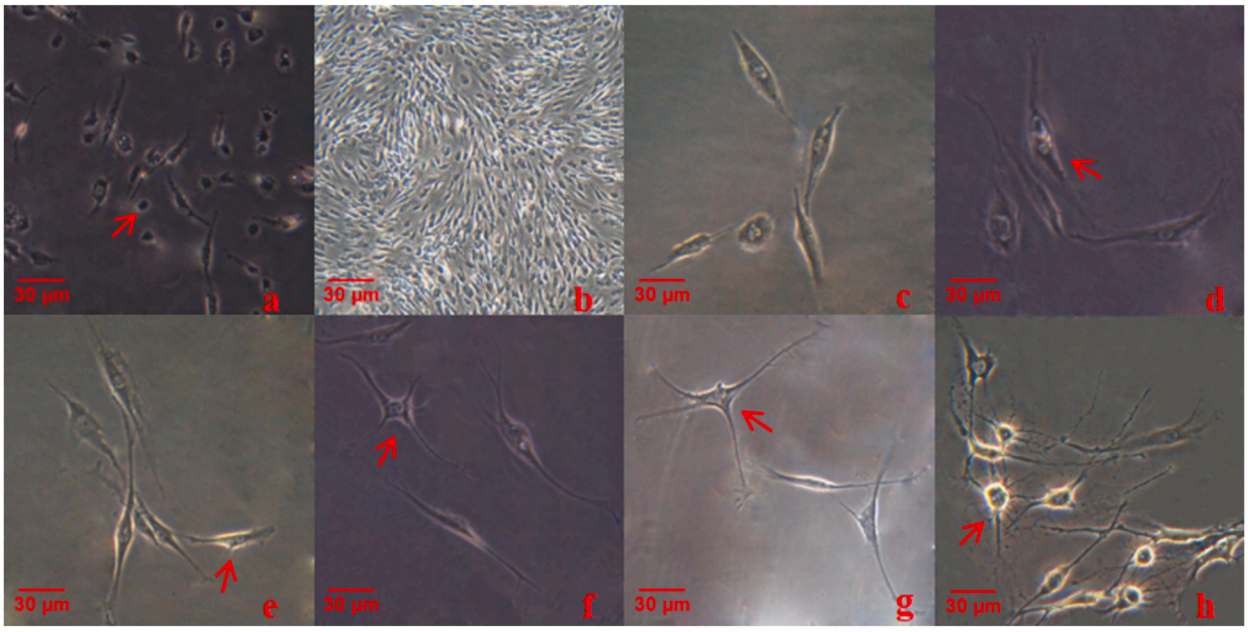

Fig. 1. Morphological features of differentiated cells after ADSCs induction reaction (inverted contrast microscopy, a–b: original magnification × 40, c–h: original magnification × 200) (a) Cells cultured for 24 h in the primary generation, arrow shows rounded cells; (b) Cells cultured for 10 days, exhibiting long spindle-shaped cells growing in a swirling pattern; (c) Cells cultured for 2 days in the third generation, displaying long spindle-shaped cells; (d) Cells pre-induced for 24 h, arrow shows an increase in the refractive power of the cells; (e) Cells induced for 1 h, arrow shows protrusions extending from the differentiated cells; (f) Cells induced for 3 h, arrow shows the morphology of differentiated cells; (g) and (h) Cells after 5 h and 8 h of induction, respectively, arrow shows a significant increase in refractoriness of the cells and longer axial protrusions extending from the cells, showing typical neuronal morphology.

2.7. Statistical analysis methods

A database for the experimental data is established using Excel 2003, and statistical analysis is performed using the SPSS 13.0 statistical software package. The data for each group are presented as mean ± standard deviation. Comparisons between different time points within the same group are conducted using one-way ANOVA, while comparisons of means between groups are performed using the SNK-q test. Statistical significance was determined for values of $P < 0.05$.

3. Result

3.1. Morphological changes in ADSCs during neuronal differentiation in vitro

ADSCs isolated and extracted from adipose tissue were fully adherent at 24 h. Under an inverted phase-contrast microscope, the cells displayed various shapes, including short spindle, long spindle, round-like, triangular, or irregular forms (Fig. 1a). After adherence, the cells began to proliferate and their morphology became more uniform. By day 7 of the culture, numerous long spindle-shaped cells were observed growing in a vortex pattern. By days 10–14, the cells reached 70%–80% confluence, and cell passaging was performed (Fig. 1b). Passages 3–5 show uniform long spindle shapes and rapid proliferation, and underwent pre-induction and formal induction reactions (Fig. 1c). The differentiation rate of cells in the uninduced group (5th day of culture of 3rd to 5th passage ADSCs) was 1.38%, in the pre-induction group was 4.93% (cells underwent differentiation, extending short protrusions with few in number, Fig. 1d), in the 1 h formal induction group was 48.67% (cell nuclei enlarged and rounded, cytoplasm retracted, long protrusions similar to neuronal axon-like structures extended around the cell body, Fig. 1e), in the 3 h group was 72.28% (increased refractivity of the cytoplasm, obvious halo visible around the cell, further elongation and increased number of protrusions intertwining into a net-like structure, Fig. 1f), in the 5 h group was 87.14% (further increased refractivity, clear halo around the cell, branching at the ends of protrusions similar to dendritic cells, and cells showing typical neuronal morphology, Fig. 1g), and in the 8 h group was 86.58% (partial retraction of the cell body, shortening and reduction in the number of protrusions around the cell body, and a significant increase in the number of dead cells compared to the 5 h group, Fig. 1h). The difference in neuronal differentiation rates between 5 and 8 h induction groups was not statistically significant ($P = 0.45$), while there were significant statistical differences between other time groups ($P < 0.05$).

3.2. Immunocytochemistry detection of the expression of NSE/GPR94/CHOP/Fas/FasL/TNFR1/TNF-α/DR5/TRAIL/Caspase8/Casoase3 during the process of ADSCs induced differentiation into neurons

NSE showed no positive expression in the uninduced group. In the pre-induced group and various time groups after induction, there were positive expressions of NSE, predominantly in the cytoplasm and protrusions of the cells. The positive cell rate in the 3 h induced group was higher than in the 1 h group ($P = 0.00$), and the 5 h group was higher than the 3 h group ($P = 0.00$), with no significant difference between the 5 h and 8 h groups ($P = 0.70$). GRP94 was positively expressed in the uninduced group, pre-induced group, and the 1 h, 3 h, 5 h, and 8 h induced groups, with the positive expression rate gradually decreasing ($F = 358.47$, $p = 0.00$), but there was no statistical difference between the 8 h and 5 h groups ($F = 1.17$, $p = 0.29$). Positive expression of GRP94 was seen in the cytoplasm and protrusions of the cells. CHOP was positively expressed in all groups, and the positive expression rate significantly increased over time ($F = 56.21$, $p = 0.00$). Positive expression was observed in the nucleus, around the nucleus, and in the cytoplasm of the protrusions, with a notably higher expression in the nucleus compared to around the nucleus and the protrusions. Fas, FasL, TNFR1, TNF-α, DR5, TRAIL, Caspase8, and Caspase3 showed positive expression in the uninduced group. The positive rates of Fas, FasL, and Caspase8 in the 3 h group were higher than in the 1 h group (all $P = 0.00$), the 5 h group was higher than the 3 h group (all $P = 0.00$), and the 8 h group was higher than the 5 h group (all $P = 0.00$). The positivity rates of TNFR1, TNF-α, DR5, and TRAIL in the 3 h group were higher than in the 1 h group (all $P = 0.00$), the 5 h group was higher than the 3 h group (all $P = 0.00$), but lower in the 8 h group

Table 1
Immunocytochemistry detection of positive cell expression rates of NSE/GRP94/CHOP/Fas/FasL/TNFR1/TNF-α/DR5/TRAIL/Caspase8/Caspase3 during ADSCs-induced differentiation into neurons (mean ± SD, n = 15).

Factors	n	uninduced	pre-induction	1 h	3 h	5 h	8 h
NSE	15	–	4.19 ± 0.53*	42.52 ± 1.73*	61.13 ± 4.51*	84.21 ± 1.51	84.52 ± 1.94
GRP94	15	65.30 ± 2.00*	64.80 ± 1.92*	55.67 ± 1.63*	45.67 ± 2.77*	35.70 ± 1.39	34.87 ± 2.77
CHOP	15	4.60 ± 1.96*	10.80 ± 1.27*	23.93 ± 1.79*	28.07 ± 1.71*	48.10 ± 3.34	49.00 ± 1.77*
Fas	15	2.80 ± 0.83*	20.22 ± 2.76*	24.79 ± 1.84*	30.93 ± 2.65*	39.08 ± 1.78	48.06 ± 2.36*
FasL	15	2.70 ± 0.57*	8.84 ± 1.13*	14.89 ± 1.41*	22.19 ± 2.18*	29.45 ± 2.28	43.05 ± 2.39*
TNFR1	15	1.23 ± 0.39*	7.26 ± 1.96*	15.01 ± 1.62*	30.66 ± 3.19*	41. 22 ± 2.57	37.00 ± 1.64*
TNF-α	15	1.31 ± 0.37*	9.18 ± 1.31*	15.68 ± 1.53*	26.62 ± 3.02*	44.23 ± 3.66	37.39 ± 2.32*
DR5	15	1.17 ± 0.36*	7.59 ± 0.88*	16.84 ± 1.32*	27.48 ± 1.71*	38.33 ± 1.70	36.77 ± 1.96*
TRAIL	15	4.10 ± 1.19*	20.35 ± 3.19*	24.15 ± 1.42*	28.15 ± 1.55*	40.81 ± 3.95	38.01 ± 2.68*
Caspase8	15	1.04 ± 2.56*	2.67 ± 0.50*	7.38 ± 0.97*	13.68 ± 1.25*	30.57 ± 3.78	33.19 ± 2.06*
Caspase3	15	1.10 ± 0.23*	2.32 ± 0.85*	7.62 ± 1.45*	14.16 ± 2.35*	33.80 ± 1.38	34.32 ± 1.67

P values were determined by one-way ANOVA. *Indicates statistically significant difference compared to the induced 5 h group (*$P < 0.05$).

compared to the 5 h group (all P = 0.00). The positive rate of Caspase3 in the 3 h group was higher than in the 1 h group (P = 0.00), the 5 h group was higher than the 3 h group (P = 0.00), but there was no significant difference between the 8 h and 5 h groups (P = 0.356). The degree of positive expression of these factors was significantly higher in the cell body compared to the protrusions (Table 1).

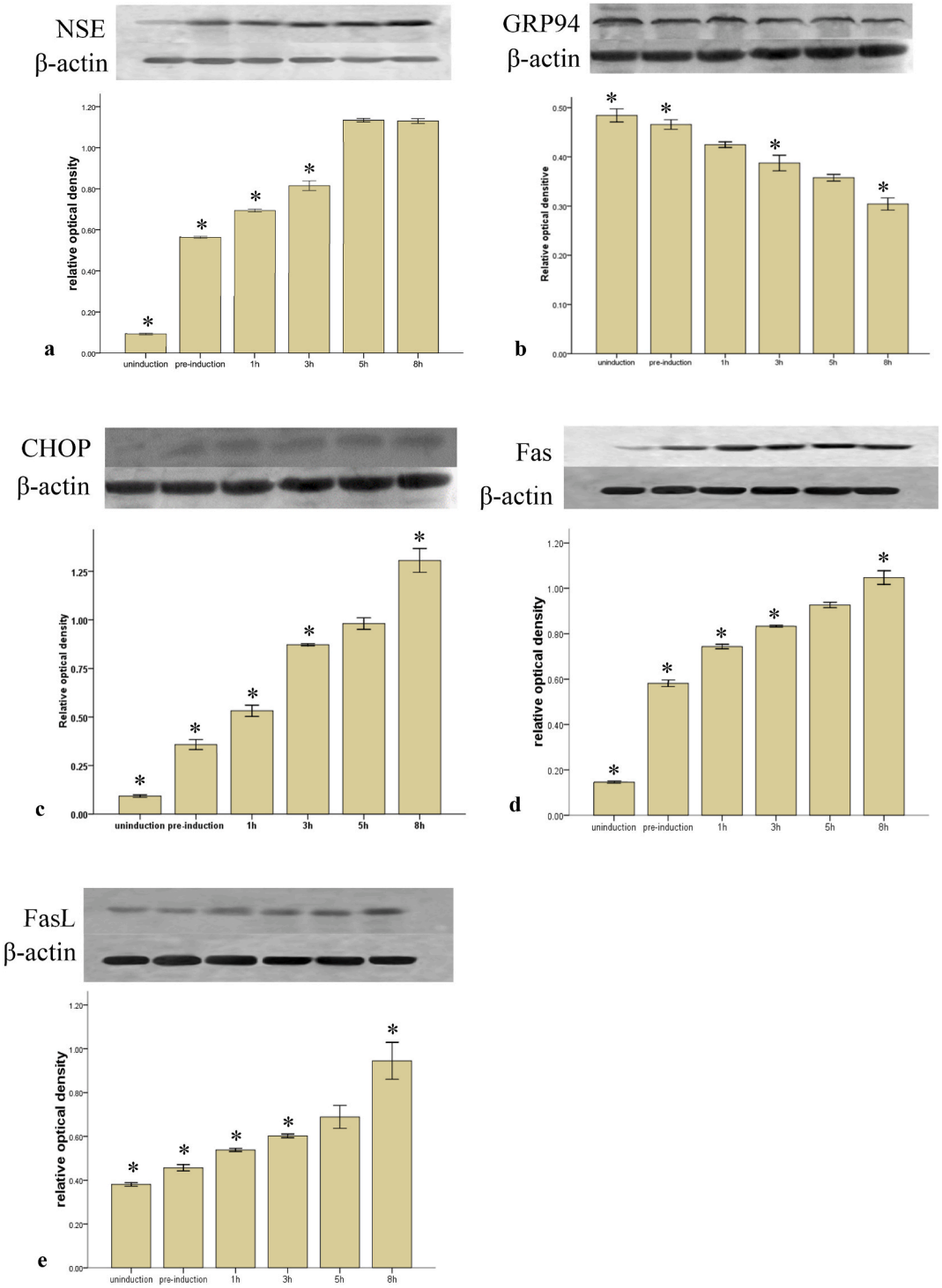

Fig. 2. Western blotting results of NSE/GPR94/CHOP/Fas/FasL/TNFR1/TNF-α/DR5/TRAIL/Caspase8/Casoase3 during the induced differentiation of ADSCs into neurons P values were determined by one-way ANOVA. *Indicates statistically significant difference compared to the induced 5 h group (*P < 0.05).

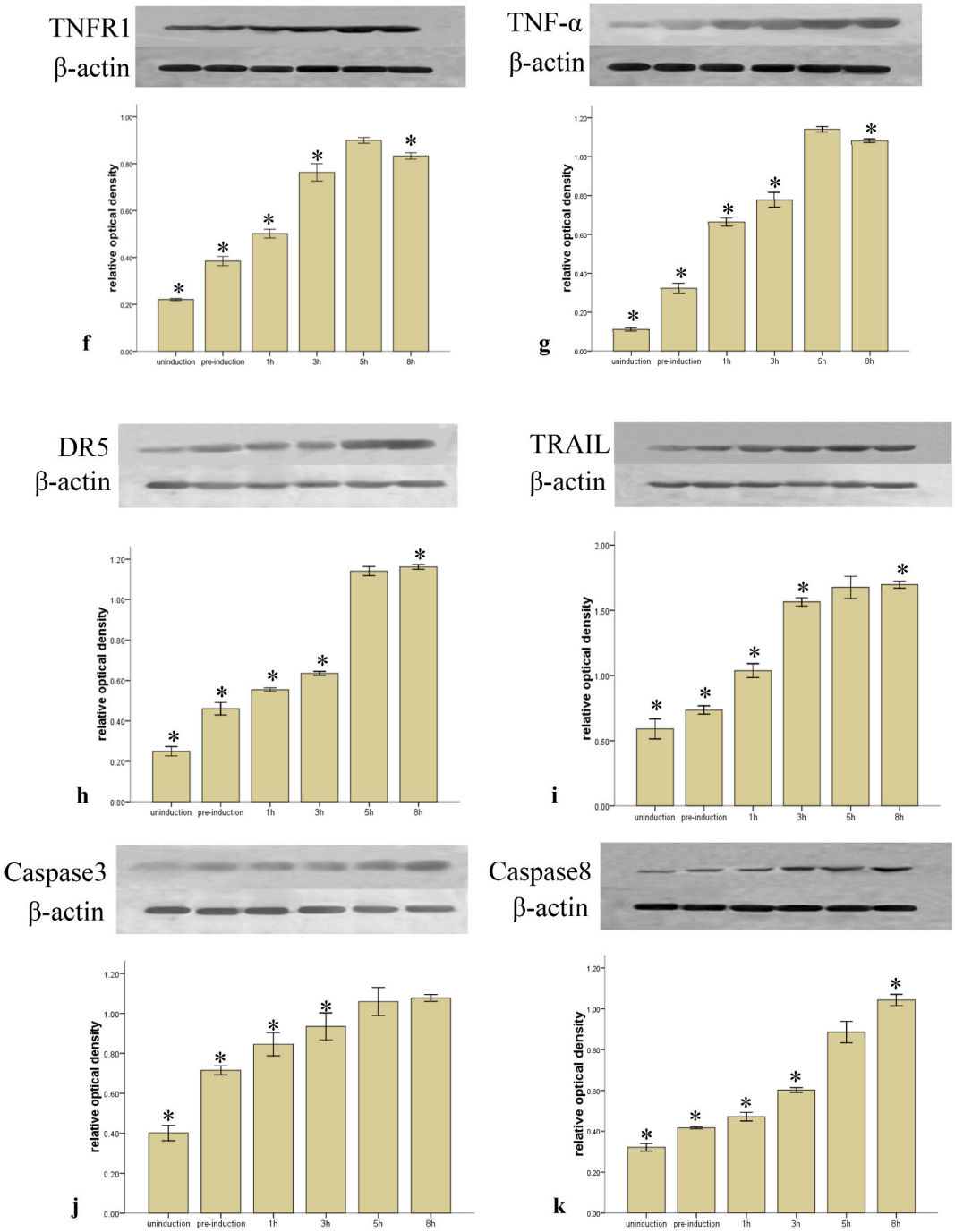

Fig. 2. (*continued*).

3.3. Western blotting results for the expression levels of NSE/GPR94/CHOP/Fas/FasL/TNFR1/TNF-α/DR5/TRAIL/Caspase8/Casoase3 during the induction of differentiation of ADSCs into neurons

There were statistically significant differences in the quantitative expression levels of NSE, GRP94, CHOP, Fas, FasL, TNFR1, TNF-α, DR5, TRAIL, Caspase8, and Caspase3 among the uninduced group, pre-induced group, and the groups induced for 1 h, 3 h, 5 h, and 8 h ($P < 0.05$). The expression level of NSE was higher in the 3 h group compared to the 1 h group ($P = 0.00$), higher in the 5 h group compared to the 3 h group ($P = 0.00$), with no significant difference between the 5 h and 8 h groups ($P = 0.556$) (Fig. 2a). The expression level of GRP94 gradually decreased with the length of induction time, reaching its lowest at 3 h ($P < 0.05$), and then

gradually increased. There was no statistical difference between the uninduced and pre-induction groups ($P > 0.05$), and between the 1 h and 5 h groups ($P > 0.05$), with statistical differences between the other groups ($P < 0.05$) (Fig. 2b). CHOP expression levels gradually increased from the uninduced, pre-induced, and 1 h, 3 h, 5 h, and 8 h induced groups, with statistically significant differences between each group ($P < 0.05$) (Fig. 2c). Fas, FasL, and Caspase8 showed increased expression levels in the 3 h group compared to the 1 h group ($P = 0.00, 0.048, 0.00$), in the 5 h group compared to the 3 h group ($P = 0.00, 0.011, 0.00$), and in the 8 h group compared to the 5 h group (all $P = 0.00$) (Fig. 2d–e and 2k). TNFR1, TNF-α, DR5, and TRAIL showed increased expression levels in the 3 h group compared to the 1 h group (all $P = 0.00$), in the 5 h group compared to the 3 h group ($P = 0.00, 0.00, 0.00, 0.015$), but decreased in the 8 h group compared to the 5 h group (all $P = 0.00$) (Fig. 2f–i). Caspase3 showed increased expression levels in the 3 h group compared to the 1 h group ($P = 0.027$), in the 5 h group compared to the 3 h group ($P = 0.005$), with no significant difference between the 5 h and 8 h groups ($P = 0.609$) (Fig. 2j) (Table 2).

3.4. Ultrastructural features of the ER in ADSCs induced to differentiate into neurons for 5 h

Under TEM, it was observed that at 5 h into the process of ADSCs being induced to differentiate into neurons, the cytoplasm of the differentiating neurons contained both normally and non-parallel arranged rough ER and Nissl bodies, which are neuron-specific organelles (Fig. 3a). In some neuronal cells, there was mild to moderate dilation of the rough endoplasmic reticulum in the cytoplasm (Fig. 3b), and even severe swelling and dilation of the endoplasmic reticulum, vacuolar changes, and degranulation were observed. Additionally, there were irregularities in the shape of the nucleus, and chromatin condensation appeared in clumps and was highly aggregated and marginalized, while the nuclear envelope remained intact (Fig. 3c).

3.5. Results of MTT assay induced differentiation of ADSCs to neuronal cells

The OD values of surviving cells showed significant statistical differences among the uninduced group (0.247 ± 0.019), pre-induced group (0.245 ± 0.018), and induced groups at 1 h (0.224 ± 0.019), 3 h (0.214 ± 0.013), 5 h (0.191 ± 0.024) and 8 h (0.136 ± 0.029) ($F = 39.331$, $P = 0.00$). There was no significant difference between the uninduced and pre-induced groups ($P = 0.832$). Similarly, there was no significant difference between the 1 h and 3 h induced groups ($P = 0.272$), while the 8 h induced group showed a significant decrease in OD values compared to the 5 h group ($P = 0.00$). The cell numbers in the 1 h, 3 h, and 5 h induced groups did not differ significantly ($P > 0.05$), indicating relatively stable cell growth during these periods (Fig. 4).

3.6. Results of the detection of apoptosis rate during the induction of differentiation of ADSCs into neurons

There were significant statistical differences in the rates of early apoptosis among the uninduced group, the pre-induced group, and the groups induced for 1 h, 3 h, 5 h, and 8 h ($F = 787.424$, $P = 0.00$). Similarly, significant differences were observed in the rates of late apoptosis among these groups ($F = 1692.066$, $P = 0.00$) (Fig. 5A–F). The rate of mechanical damage during the experiment showed no statistical differences between the pre-induced, 1 h, and 3 h groups ($F = 46.575$, $P = 0.00$) (Fig. 5B–D).

4. Discussion

Our study found that during the normal growth process of ADSCs, there is a strong unfolded protein response (UPR) triggered by ERS, leading to a relatively weak apoptotic response. However, during the process of inducing ADSCs to differentiate into neurons, UPR is significantly inhibited, and apoptosis mediated through the endoplasmic reticulum pathway is markedly enhanced, becoming a major cause of cell death. Also, in the normal growth process of ADSCs, there is a weak presence of extrinsic apoptosis mediated by death receptor pathways such as Fas/FasL, TNFR1/TNF-α, and DR5/TRAIL. Particularly noteworthy is the role of the Fas/FasL pathway as a significant mediator of apoptosis during the entire induction process, especially after 5 h of induction. The TNFR1/TNF-α

Table 2
Western-blotting detection of the relative optical density values of NSE, GRP94, CHOP, Fas, FasL, TNFR1, TNF-α, DR5, TRAIL, Caspase8, Caspase3 during ADSCs-induced differentiation into neurons (mean ± SD, n = 3).

Factors	n	uninduced	pre-induction	1 h	3 h	5 h	8 h
NSE	3	0.09 ± 0.01*	0.56 ± 0.01*	0.69 ± 0.01*	0.81 ± 0.02*	1.13 ± 0.01	1.12 ± 0.01
GRP94	3	0.48 ± 0.01*	0.47 ± 0.01*	0.43 ± 0.01	0.39 ± 0.01*	0.36 ± 0.01	0.30 ± 0.01*
CHOP	3	0.02 ± 0.00*	0.06 ± 0.00*	0.06 ± 0 0.00*	0.08 ± 0.00*	0.09 ± 0.00	0.10 ± 0.00*
Fas	3	0.14 ± 0.01*	0.58 ± 0.03*	0.74 ± 0.01*	0.83 ± 0.01*	0.92 ± 0.01	1.04 ± 0.02*
FasL	3	0.38 ± 0.01*	0.46 ± 0.01*	0.54 ± 0.01*	0.60 ± 0.01*	0.69 ± 0.05	0.94 ± 0.07*
TNFR1	3	0.22 ± 0.01*	0.38 ± 0.02*	0.50 ± 0.02*	0.76 ± 0.03*	0.89 ± 0.01	0.83 ± 0.01*
TNF-α	3	0.12 ± 0.01*	0.37 ± 0.01*	0.65 ± 0.02*	0.75 ± 0.02*	1.16 ± 0.04	1.06 ± 0.01*
DR5	3	0.21 ± 0.01*	0.48 ± 0.02*	0.57 ± 0.02*	0.65 ± 0.01*	1.33 ± 0.03	1.11 ± 0.01*
TRAIL	3	0.52 ± 0.01*	0.69 ± 0.01*	0.97 ± 0.06*	1.50 ± 0.01*	1.71 ± 0.08	1.45 ± 0.01*
Caspase8	3	0.32 ± 0.02*	0.42 ± 0.01*	0.47 ± 0.02*	0.60 ± 0.01*	0.89 ± 0.05	1.04 ± 0.02*
Caspase3	3	0.40 ± 0.03*	0.72 ± 0.02*	0.85 ± 0.05*	0.93 ± 0.06*	1.06 ± 0.06	1.08 ± 0.01

P values were determined by one-way ANOVA. *Indicates statistically significant difference compared to the induced 5 h group (*$P < 0.05$).

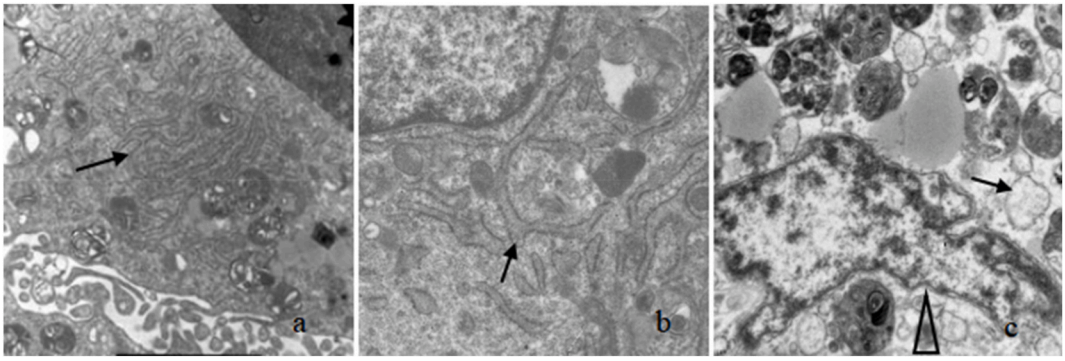

Fig. 3. Ultrastructural features of the endoplasmic reticulum of ADSCs induced to differentiate into neuronal cells for 5 h in vitro by TEM observation (a) Normal rough endoplasmic reticulum in differentiated cells at 5 h after induction, with neuron-specific organelle-Nissl body shown by arrow (original magnification × 10,000). (b) The arrow shows numerous slightly swollen rough endoplasmic reticulums around the nucleus of differentiated cells 5 h after induction (original magnification × 12000). (c) The arrow shows the enlarged lumen of the rough endoplasmic reticulum forming vacuoles and degranulation in differentiated cells that underwent apoptosis at 5 h after induction. The triangles indicate the irregular shape of the nucleus, the chromatin is concentrated and blocky, the chromatin is highly condensed and marginalized, and the nuclear membrane is intact (original magnification × 15000).

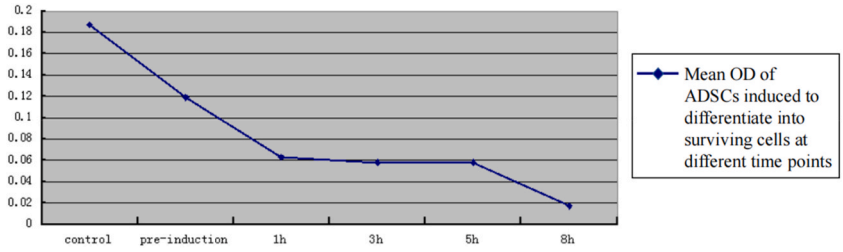

Fig. 4. MTT method to detect the results of surviving cells in the process of induced differentiation of ADSCs into neurons
Succinate dehydrogenase in the mitochondria of living cells metabolizes MTT solution to blue-purple crystals, which are dissolved in DMSO to develop the color, and the light absorbance value is measured using an enzyme marker to plot the growth curve of the cells.

and DR5/TRAIL signaling pathways also play an important role in triggering apoptosis during the first 5 h of the induction process, but their impact significantly diminishes after this period. This suggests that the death receptor-mediated apoptotic signaling pathways are significantly activated during the process of ADSC differentiation into neurons, thereby inducing apoptosis. Therefore, apoptosis mediated by the endoplasmic reticulum and death receptor pathways is a significant cause of cell death during the neuronal differentiation of ADSCs. Reducing apoptosis mediated by these two pathways can significantly improve the efficiency of the induction process.

The ER is a crucial cellular organelle involved in post-translational modification, folding, and oligomerization of proteins, as well as in lipid metabolism, synthesis of steroid hormones, and calcium storage.is involved in post-translational protein modification, folding, oligomerization, lipid metabolism, steroid hormone synthesis, and calcium storage. ERS is a physiological state that occurs when cells are exposed to various stimuli such as drugs, and radiation causing genetic damage, leading to the accumulation of unfolded or misfolded proteins in the ER, thereby impairing its function [14]. ERS can be divided into two phases: the early UPR [15] and the late phase of apoptosis induction. Through UPR, the ER can protect against cell damage caused by ER stress and restore cell function. If the damage is too severe and the internal environment cannot be promptly restored, the ER stress signals switch from promoting survival to promoting apoptosis [16]. GRP94, a hallmark protein of ERS, plays a crucial role as an ERS molecular chaperone in maintaining ER protein synthesis, proper folding, and cellular calcium homeostasis [17–20]. Therefore, during the initial phase of UPR in ERS, its expression level is relatively high, mainly as cells strive to reduce the accumulation of unfolded or misfolded proteins in the ER and attempt to restore the function and homeostasis of the ER. This phase of ERS is referred to as adaptive ERS [21,22]. Our experiment found that the expression level of GRP94 is highest in ADSCs, and it significantly decreases over time during the induction process of ADSCs differentiating into neurons. This suggests that ERS mainly plays a self-protective role during the growth of ADSCs, while this self-protective ERS is significantly weakened during the induction differentiation process. The characteristics of ER ultrastructural changes observed under the electron microscope in this study also confirm this point.

Additionally, research indicates that CHOP is a transcription factor specific to ERS and is highly sensitive to ER-mediated apoptotic responses. CHOP can induce apoptosis by activating Caspase-3, and cells lacking CHOP can tolerate apoptosis induced by ERS, thereby reflecting the level of ERS-mediated apoptosis [12,23–25]. Our results show that CHOP levels are initially low in ADSCs, but as the induction period extends, its levels significantly and progressively increase, suggesting that ERS-mediated apoptosis intensifies

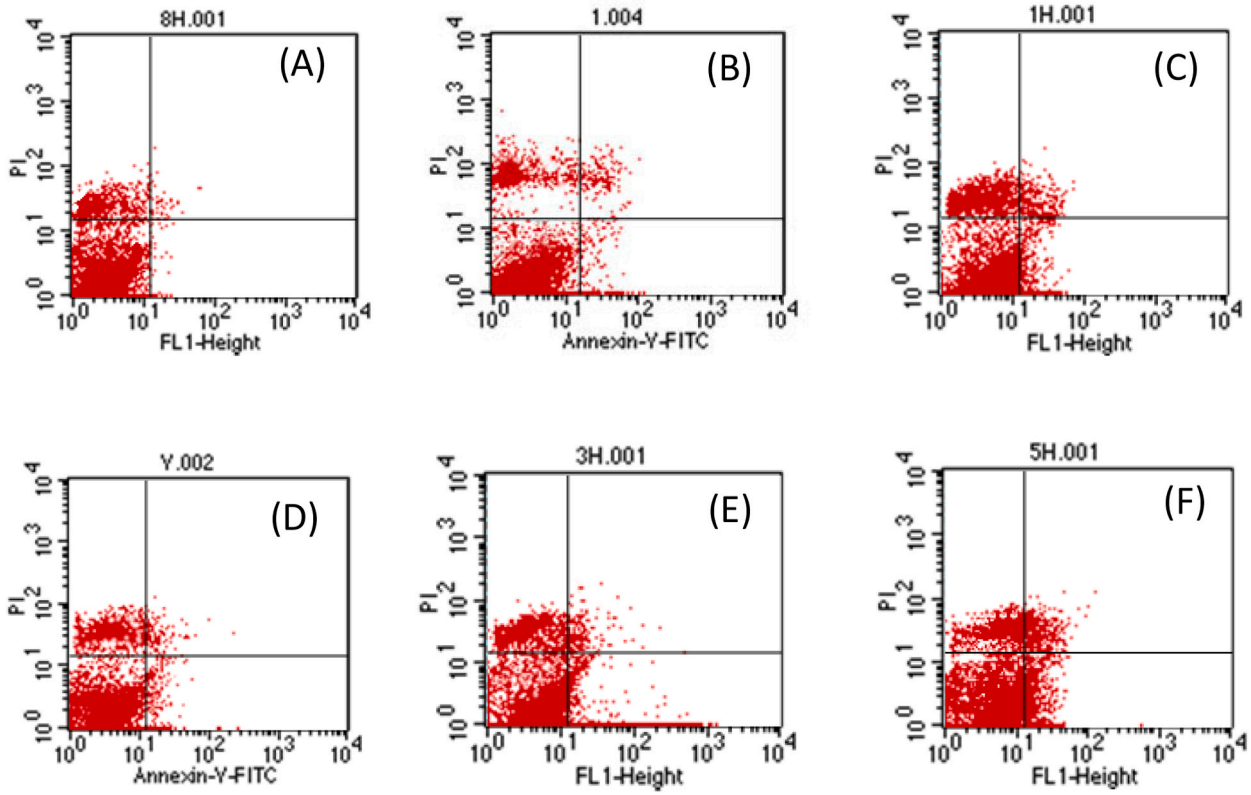

Fig. 5. Flow cytometry detection of the distribution of apoptotic cells during the induced differentiation of ADSCs to neurons
Upper left quadrant (UL): AnnexinV - PI^+ represents mechanically damaged cells; upper right quadrant (UR): $AnnexinV^+$ PI^+ represents late-apoptotic or necrotic cells; lower left quadrant (LL): AnnexinV - PI - represents of live cells; lower right quadrant (LR): Annexin V^+PI - represents early-apoptotic cells. (A) The percentages of surviving cells, early apoptotic cells, late apoptotic or necrotic cells, and mechanically damaged cells in the uninduced group were 93.22 ± 0.57%, 0.19 ± 0.05%, 0.24 ± 0.05%, and 6.17 ± 0.22%, respectively. (B) The percentages of surviving cells, early apoptotic cells, late apoptotic or necrotic cells, and mechanically damaged cells in the preinduction group were 87.75 ± 0.31%, 0.88 ± 0.12%, 1.04 ± 0.14%, and 10.53 ± 0.70%, respectively. (C) The percentage of surviving cells in the induced 1 h group was 85.38 ± 0.47%, the percentage of early apoptotic cells was 3.19 ± 0.32%, the percentage of late apoptotic or necrotic cells was 1.66 ± 0.04%, and the percentage of mechanically damaged cells was 9.60 ± 0.56%. (D) The percentages of surviving cells, early apoptotic cells, late apoptotic or necrotic cells, and mechanically damaged cells in the induced 3 h group were 83.64 ± 0.47%, 4.06 ± 0.14%, 2.08 ± 0.09%, and 10.51 ± 0.36%, respectively; (E) The percentages of surviving cells, early apoptotic cells, late apoptotic or necrotic cells, and mechanically damaged cells in the induced 5 h group were 81.11 ± 0.22% and 6.74 ± 0.21%, 3.22 ± 0.06%, and 8.63 ± 0.54%, respectively. (F) The percentages of surviving cells, early apoptotic cells, late apoptotic or necrotic cells, and mechanically damaged cells after 8 h of induction were 71.34 ± 0.91%, 12.16 ± 0.51%, 5.42 ± 0.04%, and 12.23 ± 0.61%, respectively.

throughout induction differentiation. Therefore, in ADSCs, the UPR is primarily activated, with high expression of GRP94, to maintain normal cellular functions. During the induction process, as the cells are increasingly stimulated externally, the expression level of GRP94 significantly decreases, while CHOP and Caspase-3 levels markedly increase. This indicates that with the prolongation of the induction response, the UPR caused by ERS is insufficient to maintain the stability of the internal environment of the differentiating cells, thereby initiating the ER pathway of apoptotic signaling and leading to cell death.

In the three major signaling pathways of cell apoptosis - the mitochondrial pathway, the ERS pathway, and the death receptor pathway [26–28], death receptors belong to the tumor necrosis factor receptor superfamily. They are transmembrane proteins on cells, with an extracellular part containing a cysteine-rich region and a cytoplasmic region with a “death domain (DD)" composed of homologous amino acid residues, possessing proteolytic function, acting as the initiation effector region for apoptosis mediated by this pathway [29,30]. Currently, the known death receptor-mediated apoptotic pathways mainly include Fas/FasL, TNFR1/TNF-α, and DR5/TRAIL [31]. Although these pathways differ in signal initiation, transduction, and modulation during the apoptosis process, they ultimately activate caspase8, which then activates caspase3, initiating the apoptosis response [31–34]. In our experiment, the positive expression rates and quantitative expression levels of Fas/FasL, TNFR1/TNF-α, DR5/TRAIL, Caspase8, and Caspase3 were low during the normal culture and growth of ADSCs, indicating that death receptor-mediated apoptosis was not significant at this stage. The positive rates and quantitative expression levels of Fas, FasL, and caspase8 increased with the extension of induction time, reaching peak values at the end of the 8 h induction. This suggests that the Fas/FasL pathway is an important signal transduction pathway inducing apoptosis throughout the induction process. Fas, a typical death receptor, is composed of an extracellular N-terminal

ligand-binding region, a hydrophobic transmembrane region, and a C-terminal with a DD that mediates apoptosis [35]. Its ligand, FasL, is a type II membrane protein consisting of an extracellular C-terminal ligand-binding region, a hydrophobic transmembrane region, and an intracellular region. It exists as a homotrimer complex, and its biological activity is exerted only after binding to the Fas receptor on the cell membrane [36,37]. When they bind, the DD of Fas recruits Fas-associated death domain protein (FADD) in the cytoplasm. FADD's N-terminal contains a death effector domain (DED), which recruits caspase8 to the Fas region, forming a death-inducing signaling complex (DISC) consisting of Fas, FADD, and caspase8. This activates caspase8, initiating a caspase cascade reaction, leading to apoptosis [38,39]. Analysis results from MTT and flow cytometry methods show that the cell survival rate at 5 h of induction was 81%, significantly higher than at 8 h, confirming this point.

Similarly, the DR5/TRAIL-mediated apoptotic pathway shares similarities with the Fas/FasL signaling pathway, while the TNFR1/TNF-α pathway is distinct [40–44]. The biological activity of TNF-α is primarily exerted through binding to the TNFR1 receptor on the cell membrane, inducing the recruitment of TNFR1's DD then interacts with the TNFR1-associated death domain protein (TRADD), which in turn binds with the FADD in the cytoplasm, thereby activating caspase 8 and triggering a cascade of apoptotic reactions [45–50]. Our study results show that both DR5/TRAIL/TNFR1/TNF-α signaling pathways, during the first 5 h of the induction response, exhibit a significant increase in the positive rates and expression levels of DR5, TRAIL, TNFR1, and TNF-α as the induction time extends, peaking at the 5 h mark. However, as the induction continues, their positive rates and expression levels significantly decrease. This suggests that the TNFR1/TNF-α and DR5/TRAIL-mediated apoptosis signaling pathways play an important role 5 h into the induction process, but their role in mediating apoptosis significantly weakens afterward.

Therefore, these results suggested that death receptor-mediated apoptotic signaling pathways, especially Fas/FasL, are significantly activated during the process of ADSC differentiation into neurons, thereby inducing apoptosis and becoming one of the main causes of cell death in this induction process. Additionally, flow cytometry analysis also shows that around 10% of the cells are in early and late apoptotic states at 5 h of induction, increasing to about 18% at 8 h, confirming that apoptosis is the main cause of cell death in this differentiation process. This is consistent with findings reported in other studies [10,11]. Furthermore, our flow cytometry results demonstrate that with the prolongation of the induction response, the rate of early apoptosis progressively increases, peaking at 8 h, similar to the changes observed in caspase8, a key initiator in the death receptor-mediated apoptotic pathway. This further confirms that apoptosis mediated by death receptor signaling pathways is a significant cause of cell death during the ADSC differentiation into neurons. Therefore, understanding the mechanism of apoptosis in this induction process is key to reducing cell death rates and improving the efficiency of the response.

5. Conclusion

In conclusion, ERS in the normal culture and growth of ADSCs, manifesting as enhanced UPR, maintains the normal survival of ADSCs. However, apoptosis mediated by the ERS and death receptor pathways is a significant cause of cell death in the process of ADSCs being induced to differentiate into neurons. Among these, both the ERS and the Fas/FasL pathways are important in inducing apoptosis throughout the induction process, while apoptosis mediated by the TNFR1/TNFα and DR5/TRAIL signaling pathways is particularly significant during the 5 h of the induction reaction. However, the reasons for the differential effects of these pathways require further investigation.

6. Ethics declarations

This study was reviewed and approved by the Ethics Committee of Kailuan General Hospital in Tangshan, Hebei Province, China. with the approval number: [2018010]. All patients (or their proxies/legal guardians) provided informed consent to participate in the study.

Funding statement

This work was supported by the 2020 Hebei Provincial Innovation Capacity Improvement Program–Special Project for the Construction of Science and Technology R&D Platforms and New R&D Institutions (grant number:20567622H), the 2021 Hebei Provincial Medical Science Research Project (grant number: 20210526) and the 2023 Hebei Medical Applicable Technology Tracking Project (grant number: GZ2023049).

7. Data availability statement

Data will be made available on request.

CRediT authorship contribution statement

Pingshu Zhang: Writing – review & editing, Writing – original draft, Formal analysis, Conceptualization. **Wen Li:** Writing – original draft, Methodology, Investigation, Data curation. **Xinyue Zheng:** Validation, Methodology, Investigation. **Hongjie Luo:** Software, Methodology, Investigation. **Qing Liu:** Visualization, Validation, Software. **Qingxi Long:** Visualization, Validation, Software. **Qi Yan:** Validation, Software. **Xiaodong Yuan:** Writing – review & editing, Writing – original draft, Supervision, Funding acquisition.

Declaration of competing interest

The authors declare the following financial interests/personal relationships which may be considered as potential competing interests: Yuan Xiaodong reports financial support was provided by 2020 Hebei Provincial Innovation Capacity Improvement Program. Yuan Xiaodong reports financial support was provided by 2021 Hebei Provincial Medical Science Research Project. Yuan Xiaodong reports financial support was provided by 2023 Hebei Medical Applicable Technology Tracking Project. If there are other authors, they declare that they have no known competing financial interests or personal relationships that could have appeared to influence the work reported in this paper.

Acknowledgments

Thank you to Tangshan Jinrong Beauty Hospital for contributing to the adipose tissue specimens utilized in this study. Thanks to Wu Xiaoying, Zhang Jian, Tao Li, and other Hebei Neurobiological Function Key Laboratory professors for their assistance with the experiment.

Appendix A. Supplementary data

Supplementary data to this article can be found online at https://doi.org/10.1016/j.heliyon.2024.e28608.

References

[1] P.A. Zuk, et al., Multilineage cells from human adipose tissue: implications for cell-based therapies, Tissue Eng. 7 (2) (2001) 211–228, https://doi.org/10.1089/107632701300062859.
[2] K.M. Safford, et al., Neurogenic differentiation of murine and human adipose-derived stromal cells, Biochem. Biophys. Res. Commun. 294 (2) (2002) 371–379, https://doi.org/10.1016/S0006-291X(02)00469-2.
[3] A.J. Katz, et al., Cell surface and transcriptional characterization of human adipose-derived adherent stromal (hADAS) cells, Stem Cell. 23 (3) (2005) 412–423, https://doi.org/10.1634/stemcells.2004-0021.
[4] S. Dhar, et al., Long-term maintenance of neuronally differentiated human adipose tissue–derived stem cells, Tissue Eng. 13 (11) (2007) 2625–2632, https://doi.org/10.1089/ten.2007.0017.
[5] S.K. Kang, et al., Neurogenesis of Rhesus adipose stromal cells, J. Cell Sci. 117 (Pt 18) (2004) 4289–4299, https://doi.org/10.1242/jcs.01264.
[6] S. Gao, et al., Differentiation of human adipose-derived stem cells into neuron-like cells which are compatible with photocurable three-dimensional scaffolds, Tissue Eng. 20 (7–8) (2014) 1271–1284, https://doi.org/10.1089/ten.TEA.2012.0773.
[7] C. Ye, et al., Ultrastructure of neuronal-like cells differentiated from adult adipose-derived stromal cells, Neural Regen Res 5 (2010) 1456–1463, https://doi.org/10.3969/j.issn.1673-5374.2010.19.003.
[8] Y. Lu, et al., Autophagy activator promotes neuronal differentiation of adult adipose-derived stromal cells, Neural Regen Res 8 (10) (2013) 882–889, https://doi.org/10.3969/j.issn.1673-5374.2013.10.002.
[9] X. Yuan, et al., Adult adipose-derived stromal cells differentiate into neurons with normal electrophysiological functions, Neural Regen Res 6 (34) (2011) 2681–2686, https://doi.org/10.3969/j.issn.1673-5374.2011.34.006.
[10] Q. Wang, et al., The relationship between the bcl-2/bax proteins and the mitochondria-mediated apoptosis pathway in the differentiation of adipose-derived stromal cells into neurons, PLoS One 11 (10) (2016) e0163327, https://doi.org/10.1371/journal.pone.0163327.
[11] Y. Lu, et al., Autophagy and apoptosis during adult adipose-derived stromal cells differentiation into neuron-like cells in vitro, Neural Regen Res 7 (16) (2012) 1205–1212, https://doi.org/10.3969/j.issn.1673-5374.2012.16.001.
[12] H. Hu, et al., The C/EBP homologous protein (CHOP) transcription factor functions in endoplasmic reticulum stress-induced apoptosis and microbial infection, Front. Immunol. 9 (2018) 3083, https://doi.org/10.3389/fimmu.2018.03083.
[13] M.S. Choudhery, et al., Donor age negatively impacts adipose tissue-derived mesenchymal stem cell expansion and differentiation, J. Transl. Med. 12 (2014) 8, https://doi.org/10.1186/1479-5876-12-8.
[14] H. Yoshida, ER stress and diseases, FEBS J. 274 (3) (2007) 630–658, https://doi.org/10.1111/j.1742-4658.2007.05639.x.
[15] Y. Ma, L.M. Hendershot, et al., The role of the unfolded protein response in tumour development: friend or foe? Nat. Rev. Cancer 4 (12) (2004) 966–977, https://doi.org/10.1038/nrc1505.
[16] E. Szegezdi, et al., Mediators of endoplasmic reticulum stress-induced apoptosis, EMBO Rep. 7 (9) (2006) 880–885, https://doi.org/10.1038/sj.embor.7400779.
[17] A. Eiichi, et al., Impact of endoplasmic reticulum stress pathway on pancreatic beta-cells and diabetes mellitus, Exp. Biol. Med. (Maywood, NJ, U. S.) 228 (10) (2003) 1213–1217, https://doi.org/10.1177/153537020322801018.
[18] Helene Zinszner, et al., CHOP is implicated in pror-gammed cell death in response to impaired function of the endo-plasmic reticulum, Genes Dev. 12 (7) (1998) 982–995, https://doi.org/10.1101/gad.12.7.982.
[19] X. Wang, et al., GRP94 inhabits the immortalized porcine hepatic stellate cells apoptosis under endoplasmic reticulum stress through modulating the expression of IGF-1 and ubiquitin, Int. J. Mol. Sci. 23 (22) (2022) 14059, https://doi.org/10.3390/ijms232214059.
[20] G. Zhu, A.S. Lee, et al., Role of the unfolded protein response, GRP78 and GRP94 in organ homeostasis, J. Cell. Physiol. 230 (7) (2015) 1413–1420, https://doi.org/10.1002/jcp.24923.
[21] D.T. Rutkowski, R.J. Kaufman, et al., That which does not kill me makes me stronger: adapting to chronic ER stress, Trends Biochem. Sci. 32 (10) (2007) 469–476, https://doi.org/10.1016/j.tibs.2007.09.003.
[22] P. Walter, D. Ron, et al., The unfolded protein response: from stress pathway to homeostatic regulation, Science 334 (6059) (2011) 1081–1086, https://doi.org/10.1126/science.1209038.
[23] S. Oyadomari, M. Mori, et al., Roles of CHOP/GADD153 in endoplasmic reticulum stress, Cell Death Differ. 11 (4) (2004) 381–389, https://doi.org/10.1038/sj.cdd.4401373.
[24] H. Nishitoh, CHOP is a multifunctional transcription factor in the ER stress response, J. Biochem. 151 (3) (2012) 217–219, https://doi.org/10.1093/jb/mvr143.
[25] F. Allagnat, et al., C/EBP homologous protein contributes to cytokine-induced pro-inflammatory responses and apoptosis in β-cells, Cell Death Differ. 19 (11) (2012) 1836–1846, https://doi.org/10.1038/cdd.2012.67.
[26] Krishnendu Sinha, et al., Oxidative stress: the mitochondria-dependent and mitochondria-independent pathways of apoptosis, Arch. Toxicol. 87 (7) (2013) 1157–1180, https://doi.org/10.1007/s00204-013-1034-4.

[27] L.E. French, M. Mori, et al., Protein-based therapeutic approaches targeting death receptors, Cell Death Differ. 10 (1) (2003) 117–123, https://doi.org/10.1038/sj.cdd.4401185.
[28] H. Wang, et al., Role of death receptor, mitochondrial and endoplasmic reticulum pathways in different stages of degenerative human lumbar disc, Apoptosis 16 (10) (2011) 990–1003, https://doi.org/10.1007/s10495-011-0644-7.
[29] W. H, Death receptors, Essays Biochem. 39 (2003) 53–71, https://doi.org/10.1042/bse0390053.
[30] K. Moriwaki, et al., Sweet modification and regulation of death receptor signalling pathway, J. Biochem. 169 (6) (2021) 643–652, https://doi.org/10.1093/jb/mvab034.
[31] A. Thorburn, Death receptor-induced cell killing, Cell. Signal. 16 (2) (2004) 139–144, https://doi.org/10.1016/j.cellsig.2003.08.007.
[32] X. Huang, et al., The Fas/Fas ligand death receptor pathway contributes to phenylalanine-induced apoptosis in cortical neurons, PLoS One 8 (8) (2013) e71553, https://doi.org/10.1371/journal.pone.0071553.
[33] G. Pan, et al., An antagonist decoy receptor and a death domain containing receptor for TRAIL, Science 277 (5327) (1997) 815–818, https://doi.org/10.1126/science.277.5327.815.
[34] B. Tummers, D.R. Green, et al., Caspase-8: regulating life and death, Immunol. Rev. 277 (1) (2017) 76–89, https://doi.org/10.1111/imr.12541.
[35] T. Kaufmann, et al., Fas death receptor signalling: roles of Bid and XIAP, Cell Death Differ. 19 (1) (2012) 42–50, https://doi.org/10.1038/cdd.2011.121.
[36] N. Saxena, et al., The Fas/Fas ligand apoptotic pathway is involved in abrin-induced apoptosis, Toxicol. Sci. 135 (1) (2013) 103–118, https://doi.org/10.1093/toxsci/kft139.
[37] B.J. Chang, et al., Identification of the calmodulin-binding domains of Fas death receptor, PLoS One 11 (1) (2016) e0146493, https://doi.org/10.1371/journal.pone.0146493.
[38] V.V. Saralamma, et al., Poncirin induces apoptosis in AGS human gastric cancer cells through extrinsic apoptotic pathway by up-regulation of Fas ligand, Int. J. Mol. Sci. 16 (9) (2015) 22676–22691, https://doi.org/10.3390/ijms160922676.
[39] H. Matsumura, et al., Necrotic death pathway in FAS receptor signaling, J. Cell Biol. 151 (6) (2000) 1247–1256, https://doi.org/10.1083/jcb.151.6.1247.
[40] Nils Holler, et al., Fas triggers an altermative, caepase-8-independent cell death pathway using the kinase RIP as effector molecule, Nat. Immunol. 1 (6) (2000) 489–495, https://doi.org/10.1038/82732.
[41] X. Pan, et al., Association of TRAIL and its receptors with large-artery atherosclerotic stroke, PLoS One 10 (9) (2015) e0136414, https://doi.org/10.1371/journal.pone.0136414.
[42] Jichun Sun, et al., Protective effect of RIP and c-FLIP in preventing liver cancer cell apoptosis induced by TRAIL, Int. J. Clin. Exp. Pathol. 8 (6) (2015) 6519–6525.
[43] C. Zhang, et al., TNFR1/TNF-alpha and mitochondria interrelated signaling pathway mediates quinocetone-induced apoptosis in HepG2 cells, Food Chem. Toxicol. 62 (2013) 825–838, https://doi.org/10.1016/j.fct.2013.10.022.
[44] Hsiang-Ping Lee, et al., Curcumin induces cell apoptosis in human chondrosarcoma through extrinsic death receptor pathway, Int. Immunopharm. 13 (2) (2012) 163–169, https://doi.org/10.1016/j.intimp.2012.04.002.
[45] J. Liao, et al., Electroacupuncture inhibits annulus fibrosis cell apoptosis in vivo via TNF-α-TNFR1-caspase-8 and integrin β1/Akt signaling pathways, J. Tradit. Chin. Med. 34 (6) (2014) 684–690, https://doi.org/10.1016/s0254-6272(15)30083-2.
[46] T. Yang, et al., Huachansu suppresses human bladder cancer cell growth through the Fas/Fasl and TNF- alpha/TNFR1 pathway in vitro and in vivo, J. Exp. Clin. Cancer Res. 34 (1) (2015) 21, https://doi.org/10.1186/s13046-015-0134-9.
[47] O. Micheau, J. Tschopp, et al., Induction of TNF receptor I-mediated apoptosis via two sequential signaling complexes, Cell 114 (2) (2003) 181–190, https://doi.org/10.1016/s0092-8674(03)00521-x.
[48] J.R. Townsend, et al., TNF-alpha and TNFR1 responses to recovery therapies following acute resistance exercise, Front. Physiol. 6 (2015) 48, https://doi.org/10.3389/fphys.2015.00048.
[49] L. Probert, TNF and its receptors in the CNS: the essential, the desirable and the deleterious effects, Neuroscience 302 (2015) 2–22, https://doi.org/10.1016/j.neuroscience.2015.06.038.
[50] H. Hsu, et al., The TNF receptor 1-associated protein TRADD signals cell death and NF-kappa B activation, Cell 81 (4) (1995) 495–504, https://doi.org/10.1016/0092-8674(95)90070-5.